# Combined effect of electron-electron interactions and spin-orbit scattering in metal nanoparticles

Denis A. Gorokhov and Piet W. Brouwer
*Laboratory of Atomic and Solid State Physics, Cornell University, Ithaca, New York 14853-2501, USA*
(Received 5 November 2003; published 15 April 2004)

The combined effect of electron-electron interactions and spin-orbit scattering in metal nanoparticles can be studied by measuring splitting of electron levels in magnetic field ($g$ factors) in tunneling spectroscopy experiments. Using random matrix theory to describe the single-electron states in the metal particle, we find that even a relatively small electron-electron interaction strength (ratio of exchange constant $J$ and mean level spacing $\delta \simeq 0.3$) significantly increases $g$-factor fluctuations for not-too-strong spin-orbit scattering rates (spin-orbit time $\tau_{so} \gtrsim 1/\delta$). In particular, $g$ factors larger than 2 could be observed. (This is a manifestation of the many-body correlation effects in nanoparticles). While so far measurements only on noble metal (Cu, Ag, Au) and Al samples have been done for which the effects of electron-electron interactions are negligible, we discuss the possibility of observing interaction effects in nanoparticles made of other metals.

DOI: 10.1103/PhysRevB.69.155417 PACS number(s): 73.22.−f, 72.25.Rb, 05.60.Gg, 73.23.Hk

## I. INTRODUCTION

While the study of the combined effect of electron-electron interactions and elastic impurity scattering in two dimensions and near the metal-insulator transition in three dimensions remains one of the most important problems in solid state physics, the description of electron-electron interactions in disordered normal-metal nanoparticles (i.e., ''zero dimensions'') has been found to be remarkably simple:[1,2]

At a fixed number of electrons and without spin-orbit scattering, the only relevant interaction term is a long-range exchange interaction[3]

$$H_{\rm int} = -J\mathbf{S}^2, \tag{1}$$

that couples to the total spin $\mathbf{S}$ of the nanoparticle. The exchange constant $J$ is closely related to one of the Fermi liquid constants of the bulk metal, and is independent of the details of the impurity configuration inside the nanoparticle. The interaction Hamiltonian (1), which is known as ''universal interaction Hamiltonian,'' is the only form of the electron-electron interaction compatible with random matrix theory.[2] Random matrix theory provides a valid description of single-electron states as long as the dimensionless conductance $g$ of the nanoparticle, which is the ratio of the Thouless energy $E_{\rm Th}$ and the mean level spacing $\delta$, is large.[4,5] Residual interaction terms not included in Eq. (1) are sample specific and small in comparison to Eq. (1) by, at least, a factor $1/g$.

In the presence of spin-orbit scattering, spin is also randomized, giving rise to both sample-to-sample fluctuations of the electron-electron interaction and a suppression of the exchange interaction (1). Since the spin-orbit scattering rate $\gamma_{so} = \hbar/\tau_{so}$ plays the role of a ''Thouless energy'' for the spin degree of freedom, for strong spin-orbit scattering the residual exchange interaction becomes small by a factor $\gamma_{so}/\delta \gg 1$ in comparison to the interaction strength without spin-orbit scattering. However, the exchange interaction remains the dominant contribution to the electron-electron interaction as long as $\gamma_{so}/\delta \ll g$.

In this paper, we present a detailed analysis of the combined effect of spin-orbit scattering and electron-electron interactions in the regime of moderate spin-orbit scattering, $\gamma_{so} \sim \delta$. In this parameter regime, the exchange interaction is not fully suppressed, while fluctuations are of the same order as the average.[6] This makes the regime of moderate spin-orbit scattering rates qualitatively different from that without spin-orbit scattering ($\gamma_{so} = 0$) and that of strong spin-orbit scattering ($\gamma_{so}/\delta \gg 1$.) The parameter regime $\gamma_{so} \sim \delta$ is of interest for recent experiments on metal nanoparticles,[7–10] in which the magnetic-field dependences of many-electron levels has been measured using tunneling spectroscopy.[11] Moreover, an analysis of the regime $\gamma_{so}/\delta \sim 1$ serves as a model study of the breakdown of the universal interaction Hamiltonian when the dimensionless conductance is small. A brief account of some of our findings was previously published in Ref. 12.

Experimentally, the spin structure of electronic states can be measured through the magnetic-field dependence of steps in the current-voltage characteristic of a metal nanoparticle coupled to source and drain electrodes via tunneling contacts. These steps occur if the applied voltage is equal to the difference of the energies of many-electron levels $|N_e+1;k\rangle$ and $|N_e;l\rangle$ which have $N_e$ and $N_e+1$ electrons, respectively,[13]

$$eV_{kl} = E_{N_e+1,k} - E_{N_e,l}. \tag{2}$$

The derivative $\partial V_{kl}/\partial B$ of the voltage at which a step occurs to the magnetic field $B$ is parametrized through a ''$g$ factor,''

$$e\frac{\partial V_{kl}}{\partial B} = \pm\frac{1}{2} g_{kl}\mu_B, \tag{3}$$

where $\mu_B = |e|\hbar/2mc$ is the Bohr magneton. Without spin-orbit scattering, but with electron-electron interactions, many-electron states are characterized by their total spin $S$ and by its $z$ component. Since tunneling spectroscopy measures transitions in which the electron number changes by one, the total spin $S$ of the grain changes by 1/2 upon addition or removal of an electron. This ''selection rule'' renders all observed $g$ factors equal to 2, irrespective of the spin $S_k$ and $S_l$ of the two many-electron levels participating in the transition. On the other hand, without interactions, the tunneling spectroscopy $g$ factors correspond to the magnetic

 

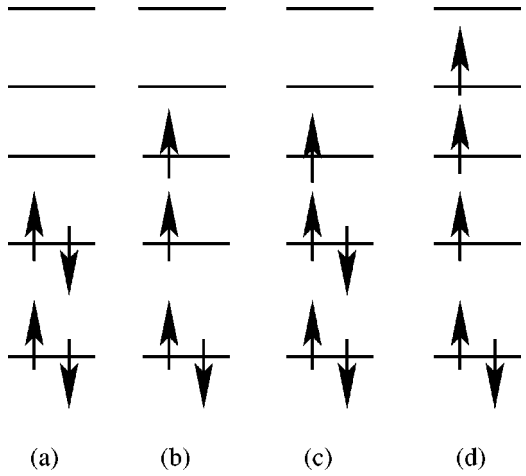


FIG. 1. Occupation of single-electron levels for the lowest-lying many-electron states with total spin $S=0$ (a) and $S=1$ (b), and for $S=1/2$ (c) and $S=3/2$ (d). In the absence of exchange interactions, the states with spin $S=0$ and $S=1/2$ are the ground states for even and odd numbers of electrons, respectively. The exchange interaction compensates (part of) the kinetic-energy cost of the higher spin states.

moment of one single-electron level only, giving rise to a distribution of $g$ factors in which all levels have, at most, spin 1/2.[14–16] As was shown in Ref. 12, the combined effect of spin-orbit scattering and electron-electron interactions is to simultaneously suppress the spin of the many-electron states and lift the selection rules, causing a much wider distribution of tunneling spectroscopy $g$ factors than in the noninteracting case. In particular, there is a significant probability to find $g$ factors larger than 2 if spin-orbit scattering is not too strong ($\gamma_{so}/\delta \lesssim 2$). The occurrence of $g$ factors larger than 2 is a unique signature of the interplay of electron-electron interactions and spin-orbit scattering.

What are the main differences between $g$-factor distributions with and without electron-electron interactions? In order to answer that question, we note that the electron-electron interactions has two main effects in a nanoparticle: to organize the many-electron states according to their total spin $S$, i.e., to lift the degeneracy between states of different $S$ but with the same orbital content, and to *lower* the energy of a many electron state with spin $S$ by the amount $JS(S+1)$, increasing the abundance of high-$S$ states among low-energy excited states, see Fig. 1. (In fact, for $J/\delta \gtrsim 0.3$, there is a significant probability that the ground state has a nontrivial spin $S>1/2$, see, e.g., Refs. 17,18.) It is because of the combination of these two effects, together with the lifting of selection rules by spin-orbit scattering, that electron-electron interactions enhance the width of the $g$-factor distribution so significantly. Moreover, because the relative abundance of high-$S$ states depends on the excitation energy, the $g$-factor distribution will be different for transitions to an excited state than for transitions to the ground states. Again, this is different from the noninteracting case, where $g$-factor distributions for transitions to the ground state and to excited states are equal. A third difference between the cases with and without interactions is that, as the selection rules are gradually broken down by spin-orbit scattering, different transitions may have very different weights, in contrast to the noninteracting case, for which all transitions have weights within a factor of order unity from each other. (The ''weight'' of the transition is the height of the corresponding step in the current-voltage characteristics.)

In principle, one should consider contributions to the $g$ factor from the orbital magnetic moments of the energy levels and from the spin magnetic moment.[15] In this work, we consider the spin contribution to the $g$ factor only and neglect the orbital contribution. For the spin-orbit scattering rates $\gamma_{so}/\delta \sim 1$ we consider here, this is justified if the electron motion in the metal grain is diffusive with mean free path $l$ much smaller than grain size $L$.[15,16]

We wish to point out that in the present paper nanoparticles of sufficiently large size and irregular shape are investigated: it is in that case only that the dimensionless conductance is large enough to justify the use of random matrix theory. For very small nanoparticles or for nanoparticles with an integrable shape random matrix theory is not applicable; in such particles shell effects may be important. Recent numerical calculations based on a tight-binding model for noninteracting electrons in an almost hemispherical Au nanoparticle with $\sim 150$ atoms have shown that even the smallest deviations from an integrable shape result in $g$ factor statistics well described by random matrix theory.[19] The inclusion of the exchange interaction in the present work does not change the applicability of random matrix theory for such nanoparticles.

The outline of this paper is as follows. In Sec. II we present the theoretical formalism. Since we only consider spin-orbit scattering rates $\gamma_{so}/\delta \ll g$, random-matrix theory can be used to describe the single-electron states. In Sec. III we discuss the results of numerical simulations for the $g$-factor distribution for transitions from the $N_e$-electron ground state to the $(N_e+1)$-electron ground state and $(N_e+1)$-electron excited states, where $N_e$ is taken even. The restriction to transitions starting from the $N_e$-electron ground state is appropriate if the metal nanoparticle relaxes to the $N_e$-electron ground state between tunneling events. In Sec. IV we discuss the consequences of our findings for various metals: our results depend on the ratio $J/\delta$, which strongly depends on the metal under consideration. We conclude in Sec. V. Finally, in the Appendix, we report an analytical calculation of the $g$-factor distribution for weak spin-orbit scattering, $\gamma_{so}/\delta \ll 1$, again paying special attention to differences between transitions involving ground states only and transitions to or from an excited state.

## II. THEORETICAL DESCRIPTION

### A. Effective Hamiltonian

Random matrix theory can be used to describe the single-electron wave functions and energy levels of a metal grain. For a metal grain with spin-orbit scattering, the appropriate random matrix ensemble interpolates between the Gaussian orthogonal ensemble (GOE) and the Gaussian symplectic ensemble (GSE) of random matrix theory,

$$H_0(\lambda)=H_{\mathrm{GOE}}+H_{\mathrm{so}}(\lambda). \tag{4}$$

Writing the spin degrees of freedom explicitly, one has

$$H_{\mathrm{GOE}}=S\otimes \mathbb{1}_2, \tag{5}$$

$$H_{\mathrm{so}}(\lambda)=\frac{i\lambda}{2\sqrt{N}}\sum_{j=1}^{3} A_j\otimes\sigma_j, \tag{6}$$

where $\mathbb{1}_2$ is the $2\times 2$ unit matrix in spin space, $\sigma_j$ is the Pauli matrix ($j=1,2,3$), $S$ is an $N\times N$ real symmetric matrices, and $A_j$ is a real antisymmetric matrix ($j=1,2,3$). The elements of the matrices $S$, $A_1$, $A_2$, and $A_3$ are drawn from independent Gaussian distributions with zero mean and with equal variances for the off-diagonal elements. The diagonal elements of $S$ have double variance, whereas the diagonal elements of $A_1$, $A_2$, and $A_3$ are zero because of the antisymmetry constraint. In random matrix theory, the limit $N\to\infty$ is taken at the end of the calculation. The random matrix description is valid as long as energy differences of the energy levels and wave functions of interest are small compared to the Thouless energy $E_{\mathrm{Th}}$.[4,5] For a disordered metal grain of size $L$, mean free path $l$, and Fermi velocity $v_F$, $E_{\mathrm{Th}}\sim v_F l/L^2$.

The parameter $\lambda$ in Eq. (4) determines the strength of the spin-orbit scattering, $\lambda^2=\pi\gamma_{\mathrm{so}}/\delta=\pi/\tau_{\mathrm{so}}\delta$, where $\tau_{\mathrm{so}}=1/\gamma_{\mathrm{so}}$ is the spin-orbit time and $\delta$ is the mean spacing between (spin-degenerate) eigenvalues of $H_{\mathrm{GOE}}$, see Refs. 14–16. The case $\lambda=0$ corresponds to the absence of spin-orbit scattering, while the limit $\lambda\to\infty$ describes the situation when spin-rotation symmetry is completely broken. The factor $1/\sqrt{N}$ in front of $H_{\mathrm{so}}$ ensures that the relation between $\lambda$ and the physical parameters $\tau_{\mathrm{so}}$ and $\delta$ does not involve the matrix size $N$.

Each eigenvalue $\varepsilon_\mu$ of the Hamiltonian (4) is doubly degenerate (Kramers degeneracy). After diagonalization, the Hamiltonian $H_0$ can be written as

$$H_0=\sum_\mu \varepsilon_\mu(\hat{\psi}^\dagger_{\mu 1}\hat{\psi}_{\mu 1}+\hat{\psi}^\dagger_{\mu 2}\hat{\psi}_{\mu 2}), \tag{7}$$

where $\hat{\psi}^\dagger_{\mu\alpha}$ and $\hat{\psi}_{\mu\alpha}$ are creation and annihilation operators for an electron in the state $|\mu\alpha\rangle$, where $\alpha=1,2$ labels the two time-reversed states in the Kramers doublet.

Combining the single-electron Hamiltonian (7) and the interaction Hamiltonian (1), one finds the total Hamiltonian

$$\hat{H}=\sum_\mu \varepsilon_\mu(\hat{\psi}^\dagger_{\mu 1}\hat{\psi}_{\mu 1}+\hat{\psi}^\dagger_{\mu 2}\hat{\psi}_{\mu 2})-J\hat{\mathbf{S}}^2. \tag{8}$$

Equation (8) is valid up to a charging energy that depends on the electron number $N_e$ only; the charging energy plays no role in the problem we consider.

In the absence of spin-orbit interaction, the exchange interaction [second term in Eq. (8)] commutes with the noninteracting Hamiltonian $H_0$ [first term in Eq. (8)]. The many-electron eigenstates are found by diagonalizing $H_0$ at a fixed value of the total spin $S$ and its $z$ component $S_z$. With spin-orbit interaction, however, the interaction does not commute with $H_0$. This has important consequences for the ground state and for the excitation spectrum of a metal grain. Typically, for most normal-metal grains and for quantum dots, $J$ is estimated to be in the range $0\lesssim J/\delta\lesssim 1$, see Sec. IV. While this implies that the effect of the exchange interaction cannot be treated in first-order perturbation theory, interaction effects only cause correlations in a small window around the Fermi energy which is, in principle, available to direct numerical diagonalization. Hereto, we write the operator $\mathbf{S}$ for the total electron spin in terms of the creation and annihilation operators $\hat{\psi}^\dagger_{\mu\alpha}$ and $\hat{\psi}_{\mu\alpha}$ of the single-electron Hamiltonian $H_0$,

$$\hat{\mathbf{S}}=\sum_{\mu,\nu}\sum_{\alpha,\beta=1,2}\hat{\psi}^\dagger_{\mu\alpha}\mathbf{s}_{\mu\alpha,\nu\beta}\hat{\psi}_{\nu\beta}, \tag{9}$$

where

$$(s_i)_{\mu\alpha,\nu\beta}=\tfrac{1}{2}\langle\nu\beta|\sigma_i|\mu\alpha\rangle,\quad i=1,2,3. \tag{10}$$

The quantity of interest in our calculation is the magnetic-field dependence of the many-electron energy levels for small magnetic fields and an odd number of electrons, which is described through the $g$ factors, see Eqs. (2) and (3) above. The magnetic-field dependence arises both through the Zeeman coupling to the electron spin and through the orbital coupling to the angular momentum.[15,16] For large diffusive metal grains and for not-too-large spin-orbit scattering strengths $\tau_{\mathrm{so}}\delta\gtrsim 1$, the Zeeman coupling dominates.[15,16,19] Since the interaction effects studied here are most important for $\tau_{\mathrm{so}}\delta\sim 1$ (see below), we neglect the orbital contribution to the $g$ factors in the discussion below. For a magnetic field $\mathbf{H}$ along the $z$ axis, the Zeeman coupling to the magnetic field is described by the Hamiltonian

$$H_Z=-2\mu_B H S_3, \tag{11}$$

where the $z$ component of the total spin $S_3$ is given by Eq. (9) above.

### B. Tunneling spectroscopy

Following Ref. 13, we assume that the conductance of the tunneling contact connecting the nanoparticle to the source reservoirs is much smaller than the conductance of the contacts connecting the particle to the drain reservoir, so that the current $I$ through the grain is limited by the processes where an electron tunnels *onto* the particle. In this case, one can assume that relaxation is sufficiently fast that the nanoparticle is in the $N_e$-particle ground state $|N_E,0\rangle$ before each tunneling event. It follows that current steps occur in the current-voltage characteristic or, equivalently, a peak in the grain's differential conductance $\partial I/\partial V$, when the source-drain voltage $eV=eV_{k0}=E_{N_e+1,k}-E_{N_e,0}$, see Eq. (2). For a point contact that injects electrons into the grain at position $\mathbf{r}$, the size of the current step is proportional to the matrix element

$$w_k=|\langle N_e+1,k|\hat{\psi}^\dagger_\uparrow(\mathbf{r})|N_e,0\rangle|^2+|\langle N_e+1,k|\hat{\psi}^\dagger_\downarrow(\mathbf{r})|N_e,0\rangle|^2, \tag{12}$$

where the creation operator $\hat{\psi}^\dagger_\sigma(\mathbf{r})$ creates an electron with spin $\sigma$ in the grain at position $\mathbf{r}$. In terms of the basis of single-electron states, one has

$$\hat{\psi}^\dagger_\sigma(\mathbf{r}) = \sum_\mu \left(\hat{\psi}^\dagger_{\mu 1}\langle \mathbf{r}\sigma|\mu 1\rangle + \hat{\psi}^\dagger_{\mu 2}\langle \mathbf{r}\sigma|\mu 2\rangle\right). \tag{13}$$

In random matrix theory, the matrix element $\langle \mathbf{r}\sigma|\mu\alpha\rangle$, $\sigma = \pm 1$, is replaced by an (arbitrary) spinor in the $2N$-component vector representing the state $\mu\alpha$, $\alpha = 1,2$.

In the presence of both spin-orbit scattering and electron-electron interactions, the $N_e$-electron states $|N_e, l\rangle$ are nondegenerate for zero magnetic field if $N_e$ is even. In that case, $\partial E_l/\partial H = 0$ at $H = 0$. On the other hand, $(N_e+1)$-electron states are doubly degenerate if $N_e$ is even. These states split in a magnetic field. For small magnetic fields the splitting is linear. Hence, if $N_e$ is even, the $g$ factor $g_{kl}$ associated with voltage $V_{kl}$ at which a current steps occurs is directly related to the magnetic-field derivative of the $(N_e+1)$-electron level $|N_e+1, l\rangle$,

$$\frac{\partial E_{N_e+1,k}}{\partial B} = \pm\frac{1}{2} g_{k0}\mu_B, \quad N_e \text{ even}. \tag{14}$$

In the remainder of this paper we continue to refer to the even-electron ground state as the "$N_e$-electron ground state" and to the odd-electron states as the "$(N_e+1)$-electron states."

An example showing how the various degeneracies are lifted by the exchange interaction and by a magnetic field is shown in Fig. 2. The top panel of the figure shows the four lowest many-electron states for an odd number of electrons, for the specific case that the ground state has spin $S = 1/2$ and the lowest excited state has $S = 3/2$ in the absence of spin-orbit scattering. Without spin-orbit scattering, the $S = 3/2$ state is fourfold degenerate. Spin-orbit scattering lifts the fourfold degeneracy of the $S = 3/2$ quadruplet, separating it into two doublets with ill-defined spin (lower panel of Fig. 2, center). Finally, an applied magnetic field lifts the degeneracy of all doublets. For an even-electron number, spin-orbit scattering lifts all possible degeneracies; to first order in the field, the applied magnetic field has no effect.

The definition that $g$ factors are derivatives of energy levels to the magnetic field implies that the Zeeman energy scale is the smallest nonzero energy scale in the problem. In particular, it is smaller than the spin-orbit induced splittings of high-spin states (see Fig. 2), these splittings being proportional to the spin-orbit scattering rate $\lambda^2 \propto 1/\tau_{so}$. However, when $g$ factors are calculated without spin-orbit scattering, the Zeeman energy is (by definition) larger than the spin-orbit rate. We'll find below that the two limits do not commute in the presence of electron-electron interactions, i.e., that $g$-factor distributions calculated in the limit $\lambda \to 0+$ are different from the $g$ factors at $\lambda = 0$. (Without spin-orbit scattering all peaks in the differential conductance split with $g$ factor $g = 2$.) It should be pointed out that experiment involves finite magnetic fields, for which the Zeeman energy

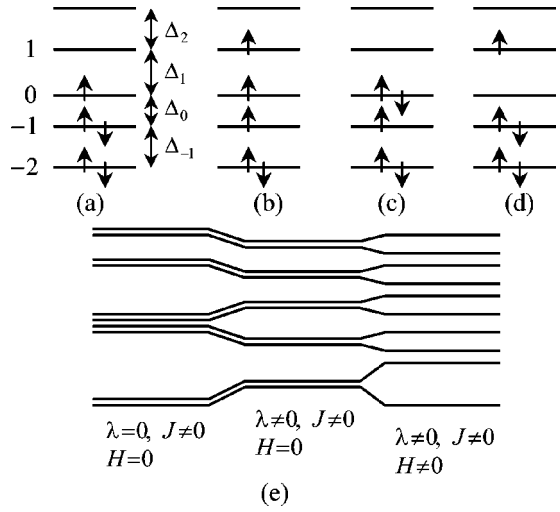


FIG. 2. Top panel: Schematic representation of four lowest many-electron levels for a grain with an odd number of particles without spin-orbit scattering. The spacings between the single-electron levels are as indicated in the figure. The figure represents the case $0 < \Delta_0 + \Delta_1 - 3J < \Delta_0, \Delta_1$. Note that the first excited state has spin $S = 3/2$ and is fourfold degenerate. Bottom panel: Evolution of energy levels of the grain for small spin-orbit scattering rates $\lambda$ and magnetic fields $H$. Spin-orbit scattering separates the quadruplet (b) into two doublets with ill-defined spin. The magnetic field lifts the degeneracy of all remaining doublets.

can be larger than the spin-orbit rate. For such magnetic-field dependences of the levels, a different slope at zero field can easily go unnoticed.

Although $g$ factors contain information on the *positions* of peaks in the tunneling spectrum of the grain, knowledge of the *sizes* of the peaks in the differential conductance is important for a correct interpretation of the results. Peak heights contain information that would be formulated in terms of selection rules in the absence of spin-orbit scattering. Indeed, without spin-orbit scattering, the total spin $S$ and its $z$ com-

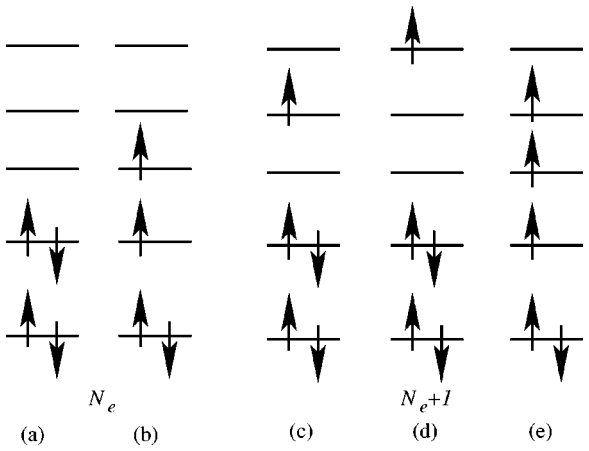


FIG. 3. Left: Schematic representation of ground states for an even number of electrons without spin-orbit scattering. Depending on the strength of the exchange interaction, the $N_e$-electron ground state may have spin $S = 0$ (a) or $S = 1$ (b). Right: three excited $(N_e+1)$-electron states.

ponent $S_3$ can change by 1/2 at most in a tunneling process, which limits the possible transitions between $N_e$ and $N_e+1$ electron states, and, hence, the possible locations of peaks in the differential conductance. It is because of the selection rules that one does not observe $g$ factors larger than 2, despite the fact that there exist high-spin many-electron states. Similarly, without interactions, the occupation of single-electron levels cannot change by more than one electron, which also limits the number of allowed transitions in tunneling spectroscopy. With spin-orbit scattering and interactions, peaks that were previously ''forbidden'' are present, in principle, although their height may be small. We return to this issue in more detail in Sec. III.

The example in Fig. 3 may further clarify the role of selection rules. The figure shows two possible $N_e$-electron ground states (left) and three $(N_e+1)$-particle excited states (right). Without spin-orbit scattering or without exchange interactions, the states (c) and (d) can be accessed from the $N_e$-particle ground state (a), but not state (e). Similarly, state (e) can be accessed from ground state (b), but not (c) and (d). When spin-orbit scattering and exchange interactions are both present, the $N_e$-electron ground state is a superposition of the states (a) and (b) and all possible transitions have a finite matrix element. Note that, since the energy difference between states (a) and (b) is typically small—on average, equal to $\delta-2J$, mixing of these two states is strong for spin-orbit scattering rates $\lambda\sim 1$.

### C. Matrix elements of interaction Hamiltonian

For the construction of the interaction Hamiltonian in the basis of many-electron eigenstates of the Hamiltonian $H_0$, one needs explicit equations for the matrix elements of the exchange interaction in that basis. Since the exchange interaction changes the single-electron states of at most two electrons, the only nonzero matrix elements of the exchange interaction occur between states that can be written in the form $\hat{\psi}^\dagger_{\mu\alpha}\hat{\psi}^\dagger_{\nu\beta}|F\rangle$ and $\hat{\psi}^\dagger_{\mu'\alpha'}\hat{\psi}^\dagger_{\nu'\beta'}|F\rangle$, where $|F\rangle$ represents a certain reference noninteracting state. After some algebra one then finds

$$\begin{aligned}\langle F|\hat{\psi}_{\nu'\beta'}\hat{\psi}_{\mu'\alpha'}\mathbf{S}^2\hat{\psi}^\dagger_{\mu\alpha}\hat{\psi}^\dagger_{\nu\beta}|F\rangle &= (\delta_{\mu\alpha,\mu'\alpha'}\delta_{\nu\beta,\nu'\beta'}-\delta_{\nu\beta,\mu'\alpha'}\delta_{\mu\alpha,\nu'\beta'})\langle F|\mathbf{S}^2|F\rangle-2[\mathbf{s}_{\nu'\beta'\mu\alpha}\cdot\mathbf{s}_{\mu'\alpha,\nu\beta}-\mathbf{s}_{\mu'\alpha',\mu\alpha}\cdot\mathbf{s}_{\nu'\beta',\nu\beta}]\\ &-2\delta_{\nu\beta,\nu'\beta'}\sum_{\phi,\gamma\in F}[\mathbf{s}_{\mu'\alpha',\phi\gamma}\cdot\mathbf{s}_{\phi\gamma,\mu\alpha}-\mathbf{s}_{\mu'\alpha',\mu\alpha}\cdot\mathbf{s}_{\phi\gamma,\phi\gamma}]-2\delta_{\mu\alpha,\nu'\beta'}\sum_{\phi,\gamma\in F}[\mathbf{s}_{\mu'\alpha',\nu\beta}\cdot\mathbf{s}_{\phi\gamma,\phi\gamma}-\mathbf{s}_{\phi\gamma,\nu\beta}\cdot\mathbf{s}_{\mu'\alpha',\phi\gamma}]\\ &-2\delta_{\nu\beta,\mu'\alpha'}\sum_{\phi,\gamma\in F}[\mathbf{s}_{\nu'\beta',\mu\alpha}\cdot\mathbf{s}_{\phi\gamma,\phi\gamma}-\mathbf{s}_{\phi\gamma,\mu\alpha}\cdot\mathbf{s}_{\nu'\beta',\phi\gamma}]-2\delta_{\mu\alpha,\mu'\alpha'}\sum_{\phi,\gamma\in F}[\mathbf{s}_{\phi\gamma,\nu\beta}\cdot\mathbf{s}_{\nu'\beta',\phi\gamma}-\mathbf{s}_{\nu'\beta',\nu\beta}\cdot\mathbf{s}_{\phi\gamma,\phi\gamma}],\end{aligned}\tag{15}$$

where

$$\langle F|\mathbf{S}^2|F\rangle=\frac{3}{4}(N_e-2)-2\sum_{\phi,\gamma\in F}\sum_{\phi',\gamma'\in F}[\mathbf{s}_{\phi\gamma,\phi'\gamma'}\cdot\mathbf{s}_{\phi'\gamma',\phi\gamma}-\mathbf{s}_{\phi\gamma,\phi\gamma}\cdot\mathbf{s}_{\phi'\gamma',\phi'\gamma'}].\tag{16}$$

The summations over $\phi$ and $\gamma$ extend over all single-electron states $|\phi,\gamma\rangle$, $\gamma=1,2$, that are occupied in the state $|F\rangle$.

Similarly, matrix elements of the Zeeman energy $H_Z$ are nonzero only if many-electron states differ by not more than one electron, i.e., between states of the form $\hat{\psi}^\dagger_{\mu\alpha}|F\rangle$ and $\hat{\psi}^\dagger_{\nu\beta}|F\rangle$. For those states, one needs the matrix elements

$$\langle F|\hat{\psi}_{\nu\beta}\mathbf{S}\hat{\psi}^\dagger_{\mu\alpha}|F\rangle=\mathbf{s}_{\nu\beta,\mu\alpha}+\delta_{\nu\beta,\mu\alpha}\sum_{\phi,\gamma\in F}\mathbf{s}_{\phi\gamma,\phi\gamma}.\tag{17}$$

At this point, it is important to verify the applicability of the random matrix theory. In order for random matrix to apply, summations over the Fermi sea should converge within a Thouless energy from the Fermi level. In Eqs. (15), (16), and (17), the sums of the form $\Sigma_{\phi,\gamma\in F}\mathbf{s}_{\phi\gamma,\phi\gamma}$ clearly satisfy this condition, by virtue of the equality

$$\mathbf{s}_{\phi1,\phi1}+\mathbf{s}_{\phi2,\phi2}=0,\tag{18}$$

which follows from the observation that the states $|\phi,1\rangle$ and $|\phi,2\rangle$ are time reversed. The sums of the form $\Sigma_{\phi,\gamma\in F}\mathbf{s}_{\mu\alpha,\phi\gamma}\cdot\mathbf{s}_{\phi\gamma,\nu\beta}$ also meet this condition, since the summand decreases $\propto 1/(\varepsilon_F-\varepsilon_\phi)^2$ for $\phi$ well below the Fermi level and $\mu$ and $\nu$ close to the Fermi level.[16] In the diagonal matrix element (16) the sum over $(\phi,\gamma)$ and $(\phi',\gamma')$ is logarithmically divergent as a function of the Fermi energy. This, however, has no consequences for the magnetic-field dependence of the many-electron states and the peak heights, since the divergence is for all matrix elements and simply corresponds to the overall shift of the ground-state energy. We conclude that random matrix theory can be used to access the many-electron ground state and the low-lying excited states.

## III. RESULTS AND DISCUSSION

In order to calculate $g$ factors and peak heights, we have diagonalized the Hamiltonian (8) numerically.

Our numerical procedure is as follows: We first diagonalized the noninteracting Hamiltonian $H_0$. The interaction is considered in a truncated basis of the many-electron states, taking the 92 lowest-lying many-electron eigenstates of $H_0$ for a $N_e+1$ electrons ($N_e$ even), and the 76 lowest-lying states for $N_e$ electrons. Finally, we diagonalized the truncated

interaction and found the $g$ factors of the $M=8$ lowest-lying $(N_e+1)$-electron states, and the peak heights that follow for transitions from the $N_e$-electron ground state. For the calculation of the $g$ factors we introduce a small magnetic field and calculate the magnetic-field derivative numerically. We verified that truncating the interaction Hamiltonian at the lowest lying 92 and 76 many-electron states has no effect on the final results by comparing our results to those that were obtained using a smaller basis set.

We have investigated exchange-interaction strength ranging from $J=0$ to $J=0.6\delta$ which is valid for most metals, see Sec. IV. The same parameter range should apply to quantum dots. Analysis of the Coulomb blockade peak spacing distribution[20] suggests that $J/\delta$ is between 0.3 and 0.4 in large quantum dots in a GaAs/GaAlAs heterostructure; whereas recent density-functional studies of ground-state spin distributions in ballistic quantum dots are compatible with the Hamiltonian (8) only if $J\approx 0.6\delta$, see Ref. 21.

Important changes occur within the range of exchange interactions we address here. Since the metal grain is assumed to relax to the $N_e$-particle ground state between tunneling events, the (statistical) properties of the $N_e$-particle ground state play a key role in determining the $g$-factor distribution. Without spin-orbit scattering for $J\lesssim 0.3\delta$, there is only a small probability that the $N_e$-particle ground state has spin one, and a vanishing probability that the $N_e+1$-particle ground state has spin 3/2 ($N_e$ is assumed even).[17,22] The probability to find an $N_e$-particle ground state with $S=1$ becomes appreciable for $J\gtrsim 0.3$, whereas the probability to find an $(N_e+1)$-particle ground with spin 3/2 becomes significant for $J\gtrsim 0.5\delta$ only. For the values of $J$ we consider, states with spin $\geqslant 5/2$ do not play a role; they have been excluded from the truncated many-electron basis.

The strength of spin-orbit scattering strength $\lambda$ is taken from 0 to 2.8. Although larger spin-orbit scattering strengths do occur in metal grains,[9,10] interaction effects are small at those values of $\lambda$ and the noninteracting theory of Refs. 14–16 works well.

The random matrices in our simulation are taken of size $2N=400$. This ensures that the condition $\lambda^2 \ll N$ necessary for the applicability of the random matrix (4) is satisfied for all values of $\lambda$. For $\lambda<2$ we have taken $2N=200$ in the simulations.

### A. Average $g$ factors

We have calculated ensemble averages of the $g$ factors $\langle g_k\rangle$, $k=0,1,\ldots,M-1$ of the $M$ lowest $(N_e+1)$-electron states. Here $g_k$ is the $g$ factor corresponding to the $k$th $(N_e+1)$-electron system, $k=0,1,\ldots,M-1$. The ensemble average is taken over 300 realizations. In Fig. 4 we show the ensemble-averaged $g$ factors for the ground state and the first excited state, $\langle g_0\rangle$ and $\langle g_1\rangle$, as well as the average over all calculated $g$ factors $\langle\overline{g}\rangle$

$$\overline{g}=M^{-1}\sum_{k=0}^{M-1} g_k. \tag{19}$$

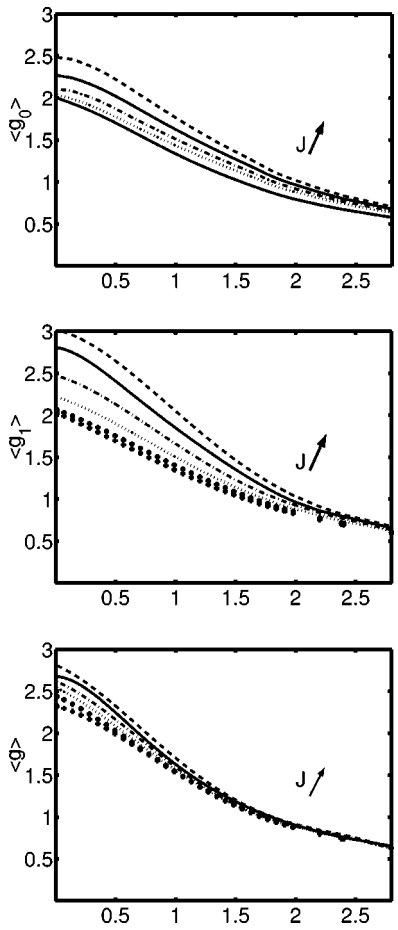


FIG. 4. Ensemble-averaged $g$ factors. Top: Average $g$ factor $\langle g_0\rangle$ of $(N_e+1)$-particle ground state for $J=0$ (the lowest solid curve), $J=0.3\delta$, $J=0.4\delta$, $J=0.5\delta$, and $J=0.6\delta$. Middle: average $g$ factor $\langle g_1\rangle$ of first excited $(N_e+1)$-particle state for $J/\delta=0.1$, 0.2, 0.3, 0.4, 0.5, and 0.6. Bottom: ensemble-averaged $g$ factor averaged over the first $M=8$ $(N_e+1)$-electron states for $J/\delta=0.1$, 0.2, 0.3, 0.4, 0.5, and 0.6.

The first observation to be made from Fig. 4 is that for $J\gtrsim 0.4\delta$ and $\lambda\lesssim 2$ interactions lead to a significant increase in the average $g$ factor. In fact, there is a significant parameter range for which $\langle\overline{g}\rangle>2$. The origin of the large $g$ factors is that exchange interactions lift the degeneracy with respect to the total spin $S$. Hence, with exchange interactions, many-electron states with a finite spin are energetically separated from states with spin 0 or 1/2. For the parameter range considered here, the relevant nontrivial spin states have $S=3/2$ for an odd number of electrons. The role of spin-orbit scattering is to lift the fourfold degeneracy of the $S=3/2$ states and, for larger spin-orbit strengths, to suppress the spin content of the single-electron states that build the many-electron state. Let us first discuss the effect of lifting the degeneracy of the $S=3/2$ state by spin-orbit scattering.

In general, spin-orbit scattering splits the fourfold degenerate $S=3/2$ state into two doublets. Neglecting contributions from other many-electron states, each doublet consist of two states that can be written in the form

$$|\text{state}\rangle = \sum_{n=-3/2}^{3/2} a_n |3/2,n\rangle, \tag{20}$$

and the time-reversed of Eq. (20), which is obtained by sending $a_n \to \text{sign}(n) a^*_{-n}$. Here $|S,S_3\rangle$ is the $(N_e+1)$-electron state with total spin $S$ and $z$ component of the spin equal to $S_3$. Because the spin-orbit matrix elements are random, the amplitudes $a_n$ are essentially random as well. (This statement is verified in the Appendix.) The $g$ factor of the state (20) is

$$g^2 = \left( \sum_{n=-3/2}^{3/2} 4n|a_n|^2 \right)^2 + \left| \sum_{n=-3/2}^{3/2} 4|n| a_n a_{-n} \right|^2. \tag{21}$$

One easily verifies that this can be larger than two. With exchange interaction but without spin-orbit scattering, there is a finite probability that the $N_e$-particle ground state ($N_e$ even) has spin $S=1$. In that case, it has two singly occupied orbitals and, hence, in principle, a finite overlap with a state of the form (20) after addition of an electron. With spin-orbit scattering, the $N_e$-electron ground state is guaranteed to be nondegenerate, so that its derivative to the magnetic field is zero. We conclude that, the $g$ factor of the state (20) can be larger than 2, that it can correspond to a transition between the $N_e$-electron ground state and an $(N_e+1)$-electron state, and that the corresponding conductance peak has a finite height.

A finite amount of spin-orbit scattering stabilizes the above arguments by increasing the splittings between many-electron states that are degenerate in the absence of spin-orbit coupling. On the other hand, with moderate spin-orbit scattering, more many-electron states are added in the doublet (20). This has two consequences: (1) the spin content of each of the underlying single-electron states is reduced, which, eventually, leads to a suppression of $g$ factors, and (2) when more many-electron states are admixed, overlaps and, hence, peak heights are increased, so that the role of selection rules is further diminished. In order to illustrate the value of $\lambda$ needed to admix different many-electron states, we note that for the $N_e$-particle ground state without spin-orbit interaction, the energy separation between the $S=1$ and $S=0$ ground states is $2J-\delta$ on average. Hence, even for a relatively small spin-orbit scattering rate $\lambda \sim 0.5$ the ground state with spin-orbit scattering will have significant weight in both of these states.

Also note that, unlike in the noninteracting case, the average $g$ factor depends on the excitation energy of the many-electron state for $\lambda \lesssim 2$, see Fig. 4. The origin of this dependence is that, without spin-orbit scattering, the probability that an $(N_e+1)$-particle state has nontrivial spin ($S \geqslant 3/2$) increases with the excitation energy. As discussed above, although spin-orbit scattering lifts the fourfold degeneracy of these states and suppresses the spin, it is the underlying nontrivial spin character persisting to finite $\lambda$ that gives rise to the increased $g$ factors.

A remarkable feature of Fig. 4 is that the ensemble-averaged $g$ factor $\langle \overline{g} \rangle$ does not approach 2 in the limit $\lambda \to 0$. On the other hand, without spin-orbit scattering, all observed $g$ factors should equal $g=2$. In Sec. II we discussed why there can be a difference between $g$ factors in the limit $\lambda \to 0$ and $g$ factors calculated without spin-orbit scattering, i.e., at $\lambda = 0$. In fact, in Fig. 4, $\langle \overline{g} \rangle$ is overestimated for $\lambda \to 0$, because the plain ensemble average does not take tunneling spectroscopy peak heights or selection rules into account: The average is taken over all $(N_e+1)$-particle states irrespective of the height of the corresponding peak in the differential conductance. In particular for small $J$, one expects that $(N_e+1)$-electron states with $g$ factors larger than 2 are likely to have small tunneling spectroscopy peak heights.

We have taken two different approaches in order to account for selection rules. First, we have replaced the ensemble average by a ''weighed'' average, in which every $g$ factor is weighed by the normalized peak height

$$\langle \overline{g} \rangle_{\text{w}} = \left\langle \sum_{k=0}^{M-1} \tilde{w}_k g_k \right\rangle, \quad \tilde{w}_k = \frac{M w_k}{\sum_{k=0}^{M-1} w_k}. \tag{22}$$

In the second approach, we have removed all peaks with normalized weight $\tilde{w}_k$ below a certain threshold value, where we arbitrarily set the threshold to $\tilde{w}_{\text{t}} = 0.1 \times \max_{k=1}^{M} w_k$,

$$\tilde{w}_k \to \tilde{w}_{k,\text{t}} = \begin{cases} 1 & \text{if } w_k \geqslant w_{\text{t}} \\ 0 & \text{if } w_k < w_{\text{t}}. \end{cases} \tag{23}$$

In this method, the number of levels per realization depends on the realization,

$$M_{\text{t}} = \sum_k \tilde{w}_{k,\text{t}}, \tag{24}$$

and the average $g$ factor is determined through

$$\langle \overline{g} \rangle = \left\langle \frac{1}{M_{\text{t}}} \sum_{k=0}^{M-1} \tilde{w}_{k,\text{t}} g_k \right\rangle. \tag{25}$$

The threshold mimics the experimental reality that small peaks cannot be distinguished from the noise, and, hence, have their $g$ factors left out in the statistical analysis. While the second method is closer to the way experiments are analyzed—all $g$ factors of conductance peaks that are observed are taken equally into account in the average—the first method has the advantage that it does not contain the somewhat arbitrary threshold at $\tilde{w}_k = \tilde{w}_{\text{t}} = 0.1$. Both methods enforce the selection rules in the absence of spin-orbit scattering. They also give almost identical results for the average $g$ factor, as is seen from Fig. 5 where we show the weighted ensemble average of the $g$ factors of all levels considered $\langle \overline{g} \rangle$, as well as the ensemble average calculated using the ''threshold'' method. As shown by comparison of Figs. 5 and 4, in the limit $\lambda \to 0$, the average $g$ factors are close to 2 for small $J$, whereas $\langle \overline{g} \rangle$ is significantly higher than 2 for $J \gtrsim 0.3$. In the inset of the lower panel of Figs. 5 we show the probability of the level to be visible, i.e., to have a peak height above the threshold. Remarkably, the curves for $J$

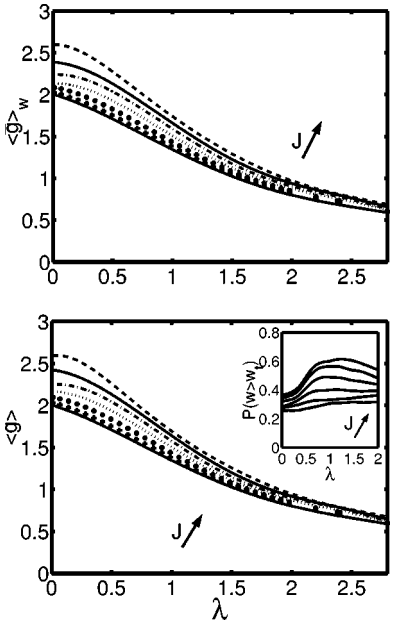


FIG. 5. Top: Average of all calculated $g$ factors, where each $g$ factor is weighed by its normalized peak height (22). Bottom: average of all calculated $g$ factors for which the normalized peak height is larger than 0.1. In both panels, results are shown for $J/\delta = 0$, 0.1, 0.2, 0.3, 0.4, 0.5, and 0.6. For $J=0$ there is no difference with Fig. 4. Inset of lower panel: the probability for a level to be visible in the experiment, i.e., to have a weight larger than the threshold one, see Eq. (23).

$\gtrsim 0.3\delta$ have a maximum for moderate values of spin-orbit scattering $\lambda \simeq 1$. This has a direct physical interpretation: both for small and large $\lambda$, approximate selection rules are in place. For small $\lambda$ these selection rules represent the conservation of spin at $\lambda = 0$, whereas for large $\lambda$ they follow from the suppression of the (exchange) interaction, which causes the remaining physics to be single-particle like.

### B. fluctuations of $g$ factors

Cumulative probability distributions of $g$ factors are shown in Fig. 6 for $J=0$, $\lambda=0.7$, for $J=0.3\delta$, $\lambda=0.7$, and for $J=0.3\delta$, $\lambda=0.9$ [we have taken into account only peaks whose weights are nonzero according to the criterion (23)]. Comparing the two distributions at $\lambda=0.7$, one notes that the exchange interaction has little effect on the tail of the $g$-factor distribution for very small $g$ factors. However, for larger $g$ factors, the weight of the probability distribution is shifted towards larger $g$ factors, including a long tail in the region $g>2$. Figure 6 confirms the previous observation that the effect of exchange interactions is to increase the average $g$ factors. The spin-orbit scattering rate for the third probability distribution shown in Fig. 6, $\lambda=0.9$, has been chosen such that the average $g$ factor $\langle \overline{g} \rangle_t \approx 1.58$ coincides with that of the case $J=0$, $\lambda=0.7$. Comparing the two probability distributions, we conclude that the interactions still lead to a significant increase of the $g$-factor fluctuations, including a large probability to find $g$ factors larger than 2, even if the average is well below 2.

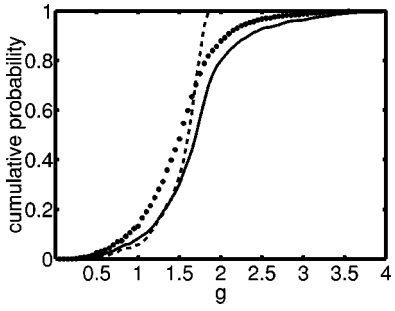


FIG. 6. Cumulative probability distributions function for $g$ factors for the cases $\lambda=0.7$, $J=0$ (dashed curve) $\lambda=0.7$, $J=0.3$ (solid), and $\lambda=0.9$, $J=0.3$ (dotted). Even a relatively small strength of the exchange interaction is enough in order to broaden the distribution function significantly.

In Fig. 7 we show the probability for a level to have a $g$ factor larger than 2. In an experiment, typically $g$ factors of 5–10 consecutive levels can be measured.[9,10] From Fig. 7 we then conclude that there is a significant probability that one of these $g$ factors is larger than 2 if $J \gtrsim 0.2\delta$. The bottom panel shows the probability that a level $|k\rangle$ has a $g$ factor larger than 2 *and* a weight $\overline{w_k} > \overline{w_t}$. As a result of the breakdown of selection rules, this probability *increases* with increasing spin-orbit scattering in the region $\lambda \lesssim 0.5$: States which have large $g$ factors but small weights for small $\lambda$ become visible for larger values of $\lambda$. The ratio of the probability shown in the bottom plot of Fig. 7 and that in the top plot of Fig. 7 is the probability that a random level can be resolved in the experiment, see Fig. 5.

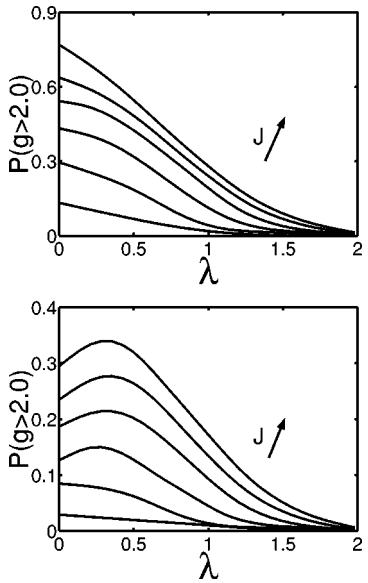


FIG. 7. Top: Probability for the $g$ factor of a level to be larger than 2.0 for the values of the exchange constant $J=0.1 \div 0.6\delta$ as a function of the spin-orbit scattering strength $\lambda$ for a random visible (i.e., satisfying the threshold criterion, see Sec. III A) level. Bottom: Probability for a random level to be visible and, at the same time, have $g>2$. for the values of the exchange constant $J=0.1 \div 0.6\delta$ as a function of the spin-orbit scattering strength $\lambda$.

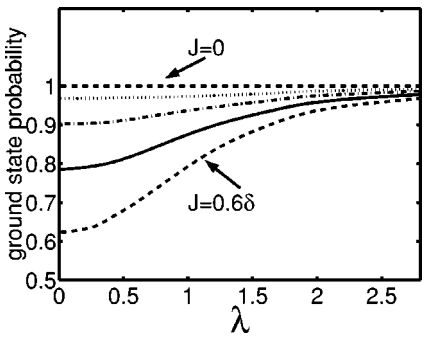


FIG. 8. Probability to be in the noninteracting ground state for $J=0.3-0.6\delta$. The horizontal line $P=1$ corresponds to the case $J=0$.

In addition to addressing the full probability distribution of $g$ factors, we should consider the possibility of correlations between $g$ factors within one realization. In principle, such correlations can exist, because, within one realization, all $g$ factors correspond to transitions from the same $N_e$-electron ground state ($N_e$ even). Although the $N_e$-electron ground state does not affect the values of all possible $g$ factors for the $(N_e+1)$-particle levels, it does affect the peak heights, and hence determines which $g$ factors possibly ''drown'' in the noise.

In order to quantify $g$-factor correlations, we have looked at the correlation function

$$C(J,\lambda)=\left\langle \sum_{k\neq l} \frac{1}{M_t^2}(g_k-\langle\overline{g}\rangle)(g_l-\langle\overline{g}\rangle)\right\rangle. \qquad (26)$$

For the calculation of the correlation function $C(J,\lambda)$ we removed all $g$ factors with normalized weight $\tilde{w}_k$ below the threshold value $\tilde{w}_t=0.1$ from the average, which means that the number levels $M_t$ considered in the summation becomes dependent on the actual realization. For the range of exchange interactions $J$ and spin-orbit scattering rates $\lambda$ we considered, the correlation function $C(J,\lambda)$ was nonzero, but always smaller than 0.1. The maximum value $C(J,\lambda)\sim 0.1$ was obtained for $\lambda\sim 0.5$. Comparing the above difference with the typical variance of $g$ factors, see Fig. 6, we conclude that correlations between different levels within the same grain are not important if the number of $g$ factors measured in a single metal nanoparticle does not exceed 10.

### C. Probability of nontrivial ground state

In Fig. 8 we show the probability that the metal grain is found in the noninteracting ground state (Fermi sea), as a function of $\lambda$ and $J$. For $N_e$-electron states, the probability to find the grain in the noninteracting ground state deviates quite significantly from 1 if $J\gtrsim 0.4$ and $\lambda=0$.[17,18] Upon increasing $\lambda$, the probability to be in the noninteracting ground state increases and approaches unity when the spin-orbit scattering rate exceeds the exchange interaction.

## IV. MATERIAL DEPENDENCE

Petta and Ralph have measured the probability distribution of $g$ factors of Cu, Au, and Ag nanoparticles.[9,10] Theoretical estimates and experimental investigations of the exchange interaction in the noble metals show that $J/\delta<0.1$ for Cu, Au, and Ag.[23,24] Hence, the interaction effects in the above materials are very small and it is natural that the existing experiments can be explained quantitatively using theory for the noninteracting ($J=0$) case. Indeed, both the average and the width of the $g$-factor probability distribution measured in Refs. 9,10 were found to be in good agreement with the noninteracting theory of Refs. 14,15 using a single fit parameter, the dimensionless spin-orbit scattering rate $\lambda$. The spin-orbit scattering time used in the fits was in order-of-magnitude agreement with previous measurements using weak localization.[25] The observation that the width of the distribution agreed well with theory after $\lambda$ has been chosen to fit the average was considered a success for random matrix theory.[26]

Significant deviations from the noninteracting theory can be expected for $J/\delta\gtrsim 0.2$ only. Although this condition is not satisfied for the noble metals, the exchange interaction is strong enough to significantly affect the $g$-factor distribution in most other metals, see Fig. 9, where a list of values of $J/\delta$ reported in the experimental and theoretical literature is given. The exchange interaction is particularly strong in Sc, V, Y, Nb, Rh, and, especially, in Pd (Pd is very close to the Stoner instability $J/\delta=1$).

For the collection of the data shown in Fig. 9, we used the fact that the ratio $J/\delta$ is related to the Fermi-liquid parameter $F_0^a$

$$J/\delta=-F_0^a, \qquad (27)$$

see Ref. 22. The Fermi-liquid parameter $F_0^a$ appears in the expression for the paramagnetic susceptibility

$$\chi=\chi_0\frac{m^*/m}{1+F_0^a}, \qquad (28)$$

where $m^*$ is the effective electron mass, including band-structure effects and interaction effects, $m$ is the free-electron mass, and $\chi_0$ is the Pauli susceptibility for free electrons,[41]

$$\chi_0=\frac{\mu_B^2 m p_F}{\pi^2\hbar^3}. \qquad (29)$$

The parameter $1/(1+F_0^a)$ is also known as the Stoner enhancement parameter.

The dimensionless spin-orbit scattering parameter $\lambda$ increases with element's nucleus charge $Z$. In experiments of Petta and Ralph[9] strong spin-orbit scattering was found for Au nanoparticles of a few nanometer in diameter ($\lambda\simeq 10$), whereas moderate spin-orbit scattering strengths ($\lambda\simeq 1$) were found in Cu and Ag nanoparticles of roughly equal size. From this, we conclude that moderate spin-orbit scattering strengths can be expected for nanoparticles with a value of $Z$

| | | | | | | | | | | | | | | | | | |
|---|---|---|---|---|---|---|---|---|---|---|---|---|---|---|---|---|---|
| 1 H | | | | | | | | | | | | | | | | | 2 He |
| 3 Li 0.23 | 4 Be 0.06–0.08 | | | | | | | | | | | 5 B | 6 C | 7 N | 8 O | 9 F | 10 Ne |
| 11 Na 0.22 | 12 Mg 0.27–0.32 | | | | | | | | | | | 13 Al −0.05–−0.2 | 14 Si | 15 P | 16 S | 17 Cl | 18 Ar |
| 19 K 0.29–0.30 | 20 Ca 0.16 | 21 Sc 0.59–0.84 | 22 Ti 0.26–0.30 | 23 V 0.57–0.63 | 24 Cr | 25 Mn | 26 Fe | 27 Co | 28 Ni | 29 Cu −0.03–0.09 | 30 Zn | 31 Ga | 32 Ge | 33 As | 34 Se | 35 Br | 36 Kr |
| 37 Rb 0.30 | 38 Sr 0.00–0.15 | 39 Y 0.53 | 40 Zr 0.16–0.20 | 41 Nb 0.39–0.42 | 42 Mo 0.13–0.19 | 43 Tc 0.24 | 44 Ru 0.25 | 45 Rh 0.41–0.44 | 46 Pd 0.84–0.89 | 47 Ag 0.02–0.07 | 48 Cd | 49 In | 50 Sn | 51 Sb | 52 Te | 53 I | 54 Xe |
| 55 Cs 0.18–0.36 | 56 Ba 0.22 | 57 La 0.52 | 72 Hf 0.18–0.20 | 73 Ta 0.36 | 74 W 0.10 | 75 Re 0.15 | 76 Os 0.17 | 77 Ir 0.29 | 78 Pt 0.59–0.72 | 79 Au 0.06 | 80 Hg | 81 Tl | 82 Pb | 83 Bi | 84 Po | 85 At | 86 Rn |
| 87 Fr | 88 Ra | 89 Ac | 104 | 105 | 106 | 107 | 108 | 109 | 110 | 111 | 112 | 113 | 114 | 115 | 116 | 117 | 118 |

FIG. 9. Ratio $J/\delta$ of the exchange-interaction constant and the mean level spacing. No value is listed for metals from $Z=24$ to 28 as they are magnetically ordered as well as all lanthanides ($Z=58,\ldots,71$) except for Pm ($Z=61$) for which no value was found in the literature. Also, for $Z>87$ no data was found in the literature. For metals in the right-hand side of the periodic table (12th column and further) only data on their Pauli susceptibility in the liquid form are available, see Ref. 27. For other metals, the data are taken from the following: Li, experiment (Ref. 24): Be, calculation of electronic structure (Refs. 28,29); Al, experiment (Ref. 30) (note the negative value of the exchange constant); K, experiments (Refs. 31,32); Ca, Y, Tc, Ba, La, Ta, W, Re, Os, Ir, calculation of electronic structure (Ref. 33); Sc, calculation of electronic structure (Refs. 33,34); Ti, Zr, Hf, calculation of electronic structure (Refs. 33,35); V, fit of theory (Ref. 36) and experiment (Ref. 37), and calculation of electronic structure (Refs. 29,33); Cu, Ag, experiment (Ref. 24) and calculation of electronic structure (Ref. 23) (note the negative exchange constant in the experiment for Cu); Rb, Cs, experiment (Ref. 31); Sr, Nb, Mo, Rh, calculation of electronic structure (Refs. 29,33); Pd, fit of theory (Ref. 36) and experiment (Ref. 38); Pt, fit of theory (Ref. 39) and experiment (Ref. 40), and calculation of electronic structure (Ref. 33); Au, calculation of electronic structure (Ref. 23).

around those for Cu or Ag. From Fig. 9 it can be seen that there are quite a few materials for which this is true and the criterion $J/\delta>0.2$ is satisfied.

## V. CONCLUSION

In this work we investigated the combined influence of electron-electron interactions and spin-orbit scattering on the $g$ factors of metal nanoparticles. In the presence of electron-electron interactions, $g$ factors must be attributed to (transitions between) many-electron states, instead of single-electron states. Many-electron states can have $g$ factors larger than 2, although these cannot be observed by tunneling spectroscopy because of selection rules as long as spin-rotation symmetry is present. Spin-orbit scattering breaks spin-rotation symmetry and thus removes the selection rules. While this leads to a suppression of the $g$ factors for large spin-orbit scattering rates, we find that $g$ factors larger than 2 occur with significant probability if the spin-orbit scattering rate $1/\tau_{so}$ is moderate, $\tau_{so}\delta\lesssim 1$, where $\delta$ is the mean spacing between single-electron energy levels in the grain. We have studied the $g$ factor distribution quantitatively using random matrix theory and the universal interaction Hamiltonian.[1,2] In addition to a confirmation of the scenario outlined above—occurrence of $g$ factors larger than 2—we found that interactions increase the width of the $g$-factor distribution for $\tau_{so}\delta \lesssim 1$ and that the $g$-factors probability distribution function is different for transitions to the odd-electron ground state and odd-electron excited states. The enhanced fluctuations occurring for moderate spin-orbit scattering strengths (spin-orbit scattering rate $\gamma_{so}$ comparable to single-electron level spacing $\delta$) may be typical of enhanced fluctuations of interaction matrix elements that are expected to occur at the breakdown of random matrix theory (dimensionless conductance $\sim 1$).

There are $\sim 20$ metallic elements in the periodic table for which the electron-electron interactions are sufficiently strong that the phenomena described here can be measured. Existing measurements of $g$ factors in nanoparticles have been made for Al and the noble metals only; in these metals, interaction effects are weak. We hope that our findings stimulate experiments on other metals.

In our calculations we have omitted the orbital contribution to the $g$ factors. The orbital contribution arises from the fact that single-electron wave functions are complex if spin-orbit scattering is present, instead of real, so that they carry a finite current density. For the parameter regime we consider here, $\tau_{so}\delta\gtrsim 1$, the single-electron wave functions are mostly real, and we expect the orbital contribution to the $g$ factor to be smaller than the spin contribution.[15,16,19] We expect that taking into account a (small) orbital contribution causes a slight increase of the average $g$ factor and a further broadening of the distribution.

## ACKNOWLEDGMENTS

We thank S. Adam, D. Huertas-Hernando, A. Kaminski, A. H. MacDonald, J. Petta, and D. C. Ralph for helpful discussions. This work was supported by the NSF under Grant No. DMR 0086509 and by the Packard foundation.

## APPENDIX: $g$ FACTORS IN THE WEAK SPIN-ORBIT SCATTERING LIMIT

In this appendix, we calculate $g$ factors to lowest order in the dimensionless spin-orbit scattering rate $\lambda$. For a state that

is twofold degenerate in the absence of spin-orbit scattering, spin-orbit scattering does not affect the spin contribution to $g$ factors up to linear order in $\lambda$.[42] Our calculation addresses the case of a fourfold degenerate level, and shows that its $g$ factor is affected to zeroth order in $\lambda$. This calculation shows explicitly that the limit $\lambda \to 0$ is singular.

Let us start by writing the spin-orbit Hamiltonian in terms of the basis of single-electron eigenstates of the Hamiltonian $H_{\mathrm{GOE}}$ without spin-orbit scattering, see Eq. (4) above,

$$H_{\mathrm{so}} = \frac{i\lambda}{2\sqrt{N}} \sum_{\mu} [(A_3)_{\mu\nu}(\hat{\psi}^{\dagger}_{\mu\uparrow}\hat{\psi}_{\nu\uparrow} - \hat{\psi}^{\dagger}_{\mu\downarrow}\hat{\psi}_{\nu\downarrow}) + (A_1 + iA_2)_{\mu\nu}\hat{\psi}^{\dagger}_{\mu\uparrow}\hat{\psi}_{\nu\downarrow} + (A_1 - iA_2)_{\mu\nu}\hat{\psi}^{\dagger}_{\mu\downarrow}\hat{\psi}_{\nu\uparrow}]. \tag{A1}$$

Here the Greek indices $\mu$ and $\nu$ refer to the eigenvalues of $H_{\mathrm{GOE}}$, and not to the eigenvalues of the total single-electron Hamiltonian $H_{\mathrm{GOE}} + H_{\mathrm{so}}$ as in Sec. II.

In order to study the effect of spin-orbit scattering on the $g$ factor of a many-electron eigenstate of $H_{\mathrm{GOE}}$ with spin $S = 3/2$, one needs to calculate matrix elements between the four members of the quadruplet. Labeling the four members of the quadruplet by the $z$ component of the spin, $S_z = p - 5/2$, $p = 1,2,3,4$, these matrix elements can be arranged in a $4 \times 4$ matrix $V$ of the form

$$V = \begin{pmatrix} -a-d & b & c & 0 \\ b^* & -a+d & 0 & c \\ c^* & 0 & -a+d & -b \\ 0 & c^* & -b^* & -a-d \end{pmatrix}, \tag{A2}$$

with $a$ and $d$ are real numbers and $b$ and $c$ represents complex numbers. The specific form of (A2) follows from time-reversal symmetry and guarantees that the eigenvalues of $V$ are double degenerate, in accordance with Kramers' theorem.

One quickly verifies that all matrix elements of $V$ are zero to first order in $H_{\mathrm{so}}$. This is the consequence of the fact that the matrices $A_j$, $j = 1,2,3$, in Eq. (A1) are antisymmetric, so that the spin-orbit interaction does not mix the states with opposite spin belonging to the same energy level. In this situation one has to calculate elements of $V$ to second order in $H_{\mathrm{so}}$.[43] Denoting the many-electron states with roman indices, the matrix elements between the many-electron states $n$ and $n'$ (both taken from the same quadruplet) are given by

$$V_{nn'} = \sum_{m} \frac{(H_{\mathrm{so}})_{nm}(H_{\mathrm{so}})_{mn'}}{E_n^{(0)} - E_m^{(0)}}, \tag{A3}$$

with $m$ is summed over all many-electron states with $E_m \neq E_n$ and $E_n^{(0)}$ and $E_m^{(0)}$ the corresponding many-electron energies.

The quadruplet state is represented schematically in Fig. 10(a). For the calculation of the splitting of a quadruplet, it is enough to consider states $m$ of the form indicated in Figs. 10(b), 10(c), and 10(d). These are: a twofold degenerate $S = 1/2$ state [Fig. 10(b)], a fourfold degenerate $S = 3/2$ state [Fig. 10(c)], and a fourfold degenerate $S = 1/2$ state [Fig. 10(d)]. There exist two variants of the states shown in Fig. 10(c) and 10(d), depending on whether an empty single-electron level is filled above the Fermi level or a hole is created below the Fermi level. The former case is shown in the figure. Since the spin-orbit interaction is a one-particle operator, only the states of the form shown in Fig. 10 which differ by not more than one electron-hole excitation are important.

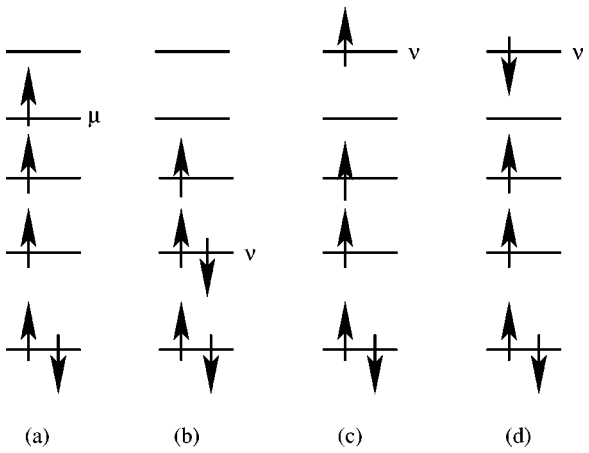


FIG. 10. An $S = 3/2$ state and the three relevant types of excited states; (a) the fourfold degenerate $S = 3/2$ ground state; (b) twofold degenerate $S = 1/2$ excited state; (c) fourfold degenerate $S = 3/2$ excited state; (d) fourfold degenerate $S = 1/2$ excited state, note that this state is entangled, see Eq. (A6).

*Virtual excitations to twofold degenerate $S = 1/2$ state.* In this case, the transition from the state $n$ to $m$ involves a transition of an electron from the singly occupied level $\mu$ to the already (singly) occupied level $\nu$, see Figs. 10(a) and 10(b). Representing the members of the spin $S = 3/2$ quadruplet as $|3/2, S_z\rangle$ with $S_z = -3/2, -1/2, 1/2, 3/2$, and the members of the spin $S = 1/2$ doublet as $|1/2, S_z\rangle$ with $S_z = 1/2, -1/2$, we find the following matrix elements of the spin-orbit Hamiltonian $H_{\mathrm{so}}$,

$$\langle 3/2, +3/2 | H_{\mathrm{so}} | 1/2, +1/2 \rangle = \frac{i\lambda}{\sqrt{4N}}(A_1 - iA_2)_{\mu\nu},$$

$$\langle 3/2, +3/2 | H_{\mathrm{so}} | 1/2, -1/2 \rangle = 0,$$

$$\langle 3/2, +1/2 | H_{\mathrm{so}} | 1/2, +1/2 \rangle = -\frac{i\lambda}{\sqrt{3N}}(A_3)_{\mu\nu},$$

$$\langle 3/2, +1/2 | H_{\mathrm{so}} | 1/2, -1/2 \rangle = \frac{i}{\sqrt{12N}}(A_1 - iA_2)_{\mu\nu},$$

$$\langle 3/2, -1/2 | H_{\mathrm{so}} | 1/2, +1/2 \rangle = -\frac{i}{\sqrt{12N}}(A_1 + iA_2)_{\mu\nu},$$

$$\langle 3/2, -1/2 | H_{\mathrm{so}} | 1/2, -1/2 \rangle = -\frac{i\lambda}{\sqrt{3N}}(A_3)_{\mu\nu},$$

$$\langle 3/2,-3/2|H_{\rm so}|1/2,+1/2\rangle = 0,$$

$$\langle 3/2,-3/2|H_{\rm so}|1/2,-1/2\rangle = -\frac{i\lambda}{\sqrt{4N}}(A_1+iA_2)_{\mu\nu}. \qquad \text{(A4)}$$

Further, in this case the energy difference

$$E_m^{(0)} - E_n^{(0)} = \varepsilon_\nu - \varepsilon_\mu + 3J. \qquad \text{(A5)}$$

Substituting these matrix elements and the energy difference into Eq. (A3) we find the following contributions to the elements of the matrix $V$ of Eq. (A2):

$$b_{1,\mu\nu} = \frac{\lambda^2 (A_1 - iA_2)_{\mu\nu}(A_3)_{\mu\nu}}{4N(\varepsilon_\nu - \varepsilon_\mu + 3J)\sqrt{3}},$$

$$c_{1,\mu\nu} = \frac{\lambda^2 (A_1 - iA_2)^2_{\mu\nu}}{4N(\varepsilon_\nu - \varepsilon_\mu + 3J)\sqrt{3}},$$

$$d_{1,\mu\nu} = \frac{\lambda^2 (A_1)^2_{\mu\nu} + \lambda^2 (A_2)^2_{\mu\nu} - 2\lambda^2 (A_3)^2_{\mu\nu}}{12N(\varepsilon_\nu - \varepsilon_\mu + 3J)}.$$

(We have not listed the value of $a$ in the matrix $V$ of Eq. (A2) since this coefficient does not contribute to the $g$ factor and splitting of the $S=3/2$ quadruplet.)

*Virtual excitations to fourfold degenerate $S=3/2$ state.* These excitations involve a transition of an electron from a singly occupied level $\mu$ to an unoccupied level $\nu$, see Fig. 10, or the transition of an electron from a doubly occupied level $\mu$ to a singly occupied level $\nu$. Calculating the various matrix elements as before, we find after somewhat cumbersome algebra

$$b_{2,\mu\nu} = -\frac{\lambda^2 (A_1 - iA_2)_{\mu\nu}(A_3)_{\mu\nu}}{6N(\varepsilon_\nu - \varepsilon_\mu)\sqrt{3}},$$

$$c_{2,\mu\nu} = -\frac{\lambda^2 (A_1 - iA_2)^2_{\mu\nu}}{6N(\varepsilon_\nu - \varepsilon_\mu)\sqrt{3}},$$

$$d_{2,\mu\nu} = -\frac{\lambda^2 (A_1)^2_{\mu\nu} + \lambda^2 (A_2)^2_{\mu\nu} - 2\lambda^2 (A_3)^2_{\mu\nu}}{18N(\varepsilon_\nu - \varepsilon_\mu)}.$$

*Virtual excitations to fourfold degenerate $S=1/2$ state.* As in the previous case, these excitations involve a transition of an electron from a singly occupied level $\mu$ to an unoccupied level $\nu$, see Fig. 10, or the transition of an electron from a doubly occupied level $\mu$ to a singly occupied level $\nu$. The four $S=1/2$ are labeled by $S_z = \pm 1/2$ and by an additional degeneracy parameter $q = \pm 1$,

$$|1/2,+1/2,q\rangle = \frac{1}{\sqrt{3}}\left(|\uparrow\uparrow\downarrow\rangle + |\uparrow\downarrow\uparrow\rangle e^{i(2\pi q/3)} + |\downarrow\uparrow\uparrow\rangle e^{-i(2\pi q/3)}\right),$$

$$|1/2,-1/2,q\rangle = \frac{1}{\sqrt{3}}\left(|\downarrow\downarrow\uparrow\rangle + |\downarrow\uparrow\downarrow\rangle e^{i(2\pi q/3)} + |\uparrow\downarrow\downarrow\rangle e^{-i(2\pi q/3)}\right). \qquad \text{(A6)}$$

Performing the calculations as before, we find

$$b_{3,\mu\nu} = \frac{\lambda^2 (A_1 - iA_2)_{\mu\nu}(A_3)_{\mu\nu}}{6N(\varepsilon_\nu - \varepsilon_\mu + 3J)\sqrt{3}},$$

$$c_{3,\mu\nu} = \frac{\lambda^2 (A_1 - iA_2)^2_{\mu\nu}}{6N(\varepsilon_\nu - \varepsilon_\mu + 3J)\sqrt{3}},$$

$$d_{3,\mu\nu} = \frac{\lambda^2 (A_1)^2_{\mu\nu} + \lambda^2 (A_2)^2_{\mu\nu} - 2\lambda^2 (A_3)^2_{\mu\nu}}{18N(\varepsilon_\nu - \varepsilon_\mu + 3J)}.$$

Denoting the set of doubly occupied single-electron levels by "0," the set of singly occupied single-electron levels by "1" and the set of unoccupied single-electron levels by "2," we then sum over all virtual excitations and find

$$b = \sum_{\mu\neq\nu\in 1} b_{1,\mu\nu} + \sum_{\mu\in 1}\sum_{\nu\in 2}(b_{2,\mu\nu} + b_{3,\mu\nu}) + \sum_{\mu\in 0}\sum_{\nu\in 1}(b_{2,\mu\nu} + b_{3,\mu\nu}), \qquad \text{(A7)}$$

and similar expressions for the coefficients $c$ and $d$ in Eq. (A2).

The matrix (A2) can be diagonalized for all values of the parameters $a$, $b$, $c$, and $d$, and the corresponding $g$ factors can be found exactly. After diagonalization we find that the quadruplet is split into two doublets with energy separation

$$(\Delta E)^2 = 4d^2 + 4|b|^2 + 4|c|^2. \qquad \text{(A8)}$$

In the $4\times 4$ matrix notation of Eq. (A2), the Zeeman Hamiltonian reads

$$H_Z = \begin{pmatrix} -3\mu_B H & & & \\ & -\mu_B H & & \\ & & \mu_B H & \\ & & & 3\mu_B H \end{pmatrix}. \qquad \text{(A9)}$$

Lifting the degeneracy of the two doublets by the Zeeman energy, we find $g$ factors

$$g = 2\sqrt{\frac{3|b|^2 + (2d \pm \Delta E)^2}{d^2 + |b|^2 + |c|^2}}, \qquad \text{(A10)}$$

where the $\pm$ sign refers to the two doublets. This result confirms the assertion made earlier, that spin-orbit scattering affects the $g$ factors of the $S=3/2$ states to zeroth order in the spin-orbit scattering rate $\lambda$. Of course, for small $\lambda$ the energy splitting $\Delta E$ is small as well, and the $g$ factor of Eq. (A10) can be observed for magnetic fields such that $\mu_B H \ll \Delta E$ only, which limits the practical observability of the $g$ factor (A10) for very small spin-orbit scattering rates $\lambda \ll 1$.

In the remainder of this appendix we investigate Eq. (A10) for the special case that one state is very close to the $S=3/2$ state of interest and virtual excitations to that state dominate the spin-orbit matrix $V$ in Eq. (A2). One important example is the case when the ground state has spin $S=3/2$, which is expected with small probability for $J/\delta \gtrsim 0.3$, see Fig. 11. Indeed, the energy difference between the $S=3/2$

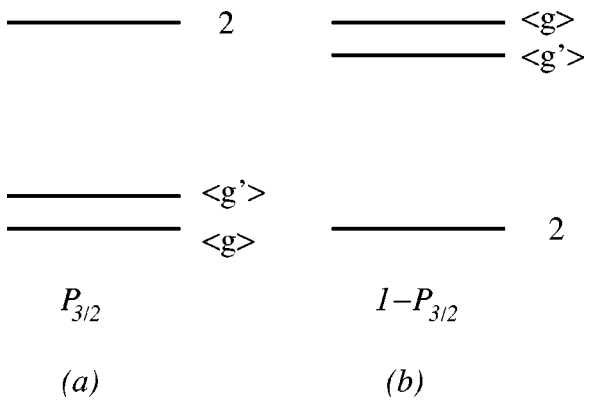


FIG. 11. Two different possibilities: (a) $S=3/2$ state is the ground state with the probability $P_{3/2}$; (b) $S=1/2$ state is the ground state with the probability $1-P_{3/2}$. Note that due to the sign change in the energy denominator, see Eq. (A3) the average $g$ factors $\langle g\rangle$ and $\langle g'\rangle$ are inverted.

state and the lowest-lying $S=1/2$ state is $\varepsilon_{\lambda+2}-\varepsilon_{\lambda}-3J$, $\lambda$ being the index of the lowest singly occupied level in the $S=3/2$ state. Typically, this energy difference is small, given the small likelihood of it being positive.

Substituting the general expressions for the coefficients $b$, $c$, and $d$ into Eq. (A10) and noting that one energy denominator is much smaller than all others, we find that an $S=3/2$ quadruplet splits into two doublets with $g$ factors

$$g=2\sqrt{1+\frac{3(A_1^2+A_2^2)}{A_1^2+A_2^2+A_3^2}},$$

$$g'=\sqrt{48-3g^2}=6\sqrt{\frac{A_3^2}{A_1^2+A_2^2+A_3^2}}, \qquad \text{(A11)}$$

where we have omitted the indices referring to the levels $\mu$ and $\nu$ involved as we deal with one excited state only. If the quadruplet state is the ground state, $g$ corresponds to the lower-lying doublet.

In the special case of an $S=3/2$ ground state, Eq. (A11) shows that the $g$ factor takes values in the interval $[2,4]$ only. One has $g=2$ only if $A_1=A_2=0$. The corresponding eigenstates are $|3/2,\pm 1/2\rangle$. In the opposite case $A_3=0$, one has $g=4$ in the ground state and the corresponding eigenstates are $(\sqrt{3}/2)|3/2,\pm 3/2\rangle-(e^{2i\phi}/2)|3/2,\mp 1/2\rangle$, where $e^{-i\phi}=(A_2+iA_1)/|A_2+iA_1|$. In fact, one can find the entire probability distribution of $g$ in this case, using the fact that $A_1$, $A_2$, and $A_3$ are taken from identical and independent Gaussian distributions,

$$P(g)=\frac{1}{2\sqrt{3}}\frac{g}{\sqrt{16-g^2}}. \qquad \text{(A12)}$$

The average $g$ factor for an $S=3/2$ ground state with a nearby $S=1/2$ state is then

$$\langle g\rangle=\frac{4}{\sqrt{3}}\left(\frac{\pi}{2}-\arcsin\frac{1}{2}+\frac{\sqrt{3}}{4}\right)\approx 3.418. \qquad \text{(A13)}$$

For $J=0.6\delta$, the probability to find a ground state with $S=3/2$ is $P_{3/2}\approx 0.38$ (see Ref. 22 or Fig. 8). Since the $g$ factor is unaffected to first order in $\lambda$ if the ground state has spin 1/2, we expect the true average ground state $g$ factor to be approximately equal to

$$\langle g_0\rangle\approx 3.418P_{3/2}+2(1-P_{3/2})\approx 2.54. \qquad \text{(A14)}$$

This value is very close to that found in the numerical simulations of the ground state $g$ factor $\approx 2.5$, see Fig. 4.

The distribution of $g'$ can be found from Eqs. (A11) and (A12). One finds the particularly simple result

$$P(g')=\tfrac{1}{6}, \quad 0<g'<6. \qquad \text{(A15)}$$

The average $\langle g'\rangle=3$. In the limiting cases $g'=6$ and $g'=0$ the doubly degenerate eigenstates have the form $|3/2,\pm 3/2\rangle$ and $(1/2)|3/2,\pm 3/2\rangle-(\sqrt{3}/2)e^{2i\phi}|3/2,\mp 1/2\rangle$, respectively. We can use these results to calculate the average $g$ factors of the lowest excited states. For the first excited state

$$\langle g_1\rangle=\langle g'\rangle P_{3/2}+\langle g'\rangle(1-P_{3/2})=\langle g'\rangle=3, \qquad \text{(A16)}$$

where we assumed that without spin-orbit scattering the ground state has spin $S=3/2$ or the first excited state has spin $S=3/2$ and is slightly below an $S=1/2$ doublet, see Fig. 11. (Hence, we neglect the possibilities that the first excited state has spin $S=1/2$ or that the first excited state has spin $S=3/2$ and is far away from the next $S=1/2$ state. Our approximation should slightly overestimate $\langle g_1\rangle$.) The simulations give $\langle g_1\rangle\approx 3.00$, see Fig. 4. With the same approximations, we find that the average $g$ factor of the second excited many-electron state is

$$\langle g_2\rangle=2P_{3/2}+\langle g\rangle(1-P_{3/2})\approx 2.87. \qquad \text{(A17)}$$

The result of the simulation is 2.78, in good agreement with the estimate (A17). Note that the above nontrivial distributions of $g$ factors can be observed in a small magnetic field only ($\mu_B H\ll\lambda^2\delta$). For larger fields the $g$ factors are the same as in the absence of spin-orbit coupling.

[1] I.L. Kurland, I.L. Aleiner, and B.L. Altshuler, Phys. Rev. B **62**, 14 886 (2002).

[2] I.L. Aleiner, P.W. Brouwer, and L.I. Glazman, Phys. Rep. **358**, 309 (2002).

[3] In principle, there is one more contribution to the interaction Hamiltonian. This is a "pairing interaction," which, if attractive, causes a superconducting instability at sufficiently low temperatures. We consider normal-metal nanoparticles for which the pairing interaction is small.

[4] K.B. Efetov, Adv. Phys. **32**, 53 (1983).

[5] B.L. Altshuler and B.I. Shklovskii, Zh. Eksp. Teor. Fiz. **91**, 220 (1986) [Sov. Phys. JETP **64**, 127 (1986)].

[6] S. Adam, P.W. Brouwer, J.P. Sethna, and X. Waintal, Phys. Rev. B **66**, 165310 (2002).
[7] D.G. Salinas, S. Guéron, D.C. Ralph, C.T. Black, and M. Tinkham, Phys. Rev. B **60**, 6137 (1999).
[8] D. Davidovic and M. Tinkham, Phys. Rev. Lett. **83**, 1644 (1999).
[9] J.R. Petta and D.C. Ralph, Phys. Rev. Lett. **87**, 266801 (2001).
[10] J.R. Petta and D.C. Ralph, Phys. Rev. Lett. **89**, 156802 (2002).
[11] D.C. Ralph, C.T. Black, and M. Tinkham, Phys. Rev. Lett. **74**, 3241 (1995).
[12] D.A. Gorokhov and P.W. Brouwer, Phys. Rev. Lett. **91**, 186602 (2003).
[13] J. von Delft and D.C. Ralph, Phys. Rep. **345**, 61 (2001).
[14] P.W. Brouwer, X. Waintal, and B.I. Halperin, Phys. Rev. Lett. **85**, 369 (2000).
[15] K.A. Matveev, L.I. Glazman, and A.I. Larkin, Phys. Rev. Lett. **85**, 2789 (2000).
[16] S. Adam, M. Polianski, X. Waintal, and P.W. Brouwer, Phys. Rev. B **66**, 195412 (2002).
[17] P.W. Brouwer, Y. Oreg, and B.I. Halperin, Phys. Rev. B **60**, 13 977 (1999).
[18] H.U. Baranger, D. Ullmo, and L.I. Glazman, Phys. Rev. B **61**, 2425 (2000).
[19] A. Cehovin, C.M. Canali, and A.H. MacDonald, Phys. Rev. B **69**, 045411 (2003).
[20] G. Usaj and H.U. Baranger, Phys. Rev. B **67**, 121308 (2003); Y. Alhassid and T. Rupp, Phys. Rev. Lett. **91**, 056801 (2003).
[21] H. Jiang, H.U. Baranger, and W. Yang, Phys. Rev. Lett. **90**, 026806 (2003).
[22] Y. Oreg, P. W. Brouwer, X. Waintal, and B. I. Halperin, in *Nano-Physics and Bio-Electronics: A New Odyssey*, edited by T. Chakraborty, F. Peeters, and U. Sivan (Elsevier, New York, 2002).
[23] A.H. MacDonald, J.M. Daams, S.H. Vosko, and D.D. Koelling, Phys. Rev. B **25**, 713 (1982).
[24] D.C. Vier, D.W. Tolleth, and S. Schultz, Phys. Rev. B **29**, 88 (1984).
[25] G. Bergmann, Phys. Rep. **107**, 1 (1984).
[26] In the analysis of Refs. 9, 10, the orbital contribution to the $g$ factors was omitted. Omitting the orbital contribution is questionable for grains in which small $g$ factors are measured ($g \sim 0.2$), since the orbital contribution to the $g$ factor is predicted to saturate around $g \sim 1$ for strong spin-orbit scattering in ballistic nanoparticles (Ref. 15).
[27] R. Dupree and D.J.W. Geldart, Solid State Commun. **9**, 145 (1971).
[28] L. Wilk, W.R. Fehlner, and S.H. Vosko, Can. J. Phys. **56**, 266 (1978).
[29] J.F. Janak, Phys. Rev. B **16**, 255 (1977).
[30] G.L. Dunifer, M.R. Pattison, and T.M. Hsu, Phys. Rev. B **15**, 315 (1977).
[31] B. Knecht, J. Low Temp. Phys. **21**, 619 (1975).
[32] D.L. Randles, Proc. R. Soc. London, Ser. A **331**, 85 (1972).
[33] M.M. Sigalas and D.A. Papaconstantopoulos, Phys. Rev. B **50**, 7255 (1994).
[34] A.H. Macdonald, K.L. Liu, and S.H. Vosko, Phys. Rev. B **16**, 777 (1977).
[35] I. Bakonyi, H. Ebert, and A.I. Liechtenstein, Phys. Rev. B **48**, 7841 (1993).
[36] E. Stenzel and H. Winter, J. Phys. F: Met. Phys. **16**, 1789 (1986).
[37] D. Hechtfischer, Z. Phys. B **23**, 255 (1976).
[38] A.J. Manuel and J.M.P.S. Quinton, Proc. R. Soc. London, Ser. A **273**, 142 (1963).
[39] F.Y. Fradin, D.D. Koelling, A.J. Freeman, and T.J. Watson-Yang, Phys. Rev. B **12**, 5570 (1975).
[40] D.W. Budworth, F.E. Hoare, and J. Preston, Proc. R. Soc. London, Ser. A **257**, 250 (1960).
[41] D. Pines and P. Nozières, *The Theory of Quantum Liquids* (W. A. Benjamin, New York, 1966).
[42] J. Sone, J. Phys. Soc. Jpn. **42**, 1457 (1977).
[43] L. D. Landau and E. M. Lifshitz, *Quantum Mechanics*, Course in Theoretical Physics, Vol. 3 (Pergamon, Oxford, 1977).